# Influence of Thermal Radiation on Layered Dust Explosions\*,\*\*

Swagnik Guhathakurta<sup>a,\*,1</sup>, Ryan W. Houim<sup>a,2</sup>

<sup>a</sup>Department of Mechanical and Aerospace Engineering, University of Florida, Gainesville, FL 32611, USA

#### ARTICLE INFO

#### Keywords: layered dust explosions radiation heat transfer numerical simulations

#### ABSTRACT

Multidimensional unsteady numerical simulations were carried out to explore the influence of thermal radiation on the propagation and structure of layered coal dust explosions. The simulation solved the reactive compressible Navier-Stokes equations coupled to an Eulerian kinetictheory-based granular multiphase model. The radiation heat transfer is modeled by solving the radiation transfer equation using the third-order filtered spherical harmonics approximation. The radiation was assumed to be gray and all boundaries of the domain are black at 300 K. The reaction mechanism is based on global irreversible reactions for each physical process including devolatilization, char burning, moisture vaporization, and methane combustion. The governing equations were solved using a high-order Godunov method. Several simulation configurations were considered: layer volume fractions of 47% and 1%, channel lengths of 10 m and 40 m, and radiative and non-radiative cases. The results show that gray radiation has a significant influence on the propagation and structure of a layered dust explosion. However, radiation can have opposite effects on different scenarios. For example, radiation promotes the propagation of the dust flame when the layer volume fraction was 1% and in the short-channel cases where reflected shock-flame interactions are important. However, radiation enhances quenching for the 47% volume fraction dust layer in the longer channel.

## 1. Introduction

Dust explosions can occur when reactive particles are dispersed into a gaseous oxidizer. They can cause significant overpressures, which, in turn, may lead to severe structural damage as well as fatalities. Many common organic materials, such as powdered spices, sugar, coffee, etc., as well as non-organic materials such as powered metals (aluminum, magnesium and titanium) can be causes of dust explosions. Some recent notable incidents related to dust explosions include the Imperial Sugar Explosion in Port Wentworth, Georgia, USA (February, 2008) that caused 38 injuries and 6 fatalities, an aluminum dust explosion in Kunshan, China (August, 2014) which killed 146, and Benxihu Colliery coal mine explosion in Benxi, Liaoning, China (April, 1942), which is one of the worst coal mine accidents in recorded history that caused 1,549 fatalities. Thus, understanding dust explosions is essential to develop improved mitigation strategies and regulation, or, in the best case, completely avoid them.

Most data available on the combustion of dust clouds are obtained from experiments using closed bombs. These closed bomb experiments usually do not provide visual access and typically measure only pressure within the vessel. While the pressure-time history provides important information on the explosivity of dust clouds usually with the  $K_{\rm st}$  explosion index, fundamental knowledge on the propagation mechanism and structure of the dust flame are not obtained. In addition, dust flames and explosions are often optically thick which makes visualization of their fundamental structure difficult. As a result, comprehensive mathematical and numerical models are necessary to increase fundamental understanding of the structure and propagation mechanisms of dust explosions.

Dust explosions have a significant history of study. However, there are relatively few reports available in the literature about the effects of radiative heat transfer on the flame ignition and propagation behavior. One of the reasons that thermal radiation is often neglected can be attributed to its complexity and computational cost. In cases where radiation is considered, the optically thick approximation is typically assumed (Slezak, Buckius and Krier, 1985), which is accurate if the entire explosion is used as the characteristic length scale. However, in many cases the radiation is optically intermediate if the dust flame thickness is used as the characteristic length. In reality the radiation opacity will be somewhere in between these two limits, which makes understanding the role of radiation on dust explosions difficult

<sup>\*</sup>This document is the results of the research project funded by the National Science Foundation.

<sup>\*</sup>Corresponding author

<sup>\*\*</sup>Principal corresponding author

swagnik@ufl.edu (S. Guhathakurta); rhouim@ufl.edu (R.W. Houim)
ORCID(s): 0000-0002-2699-1311 (S. Guhathakurta)

due to the inherent nonlinearity if the optical thickness is in an intermediate regime. In such cases, the radiation transfer equation (RTE) must be solved because traditional RTE approximations based on optically thick or thin assumptions are not accurate.

Some of the only modeling work that consider radiation in explosion processes include Cao, Gao, Liang, Xu and Pan (2014), Houim and Oran (2015a), Bidabadi and Azad (2015) and Liberman, Ivanov and Kiverin (2015). While the first three concentrate on coal dust flames, the fourth article studied the effects of radiation on particle-laden hydrogen-oxygen flames. Liberman et al. (2015) assume the gas phase is transparent to radiation, whereas the particles can both absorb and emit radiation. Different effects were observed depending on how the particles were distributed in the hydrogen-oxygen suspension. The reactants ahead of the flame was preheated due to absorption of thermal radiation by the cold particles. This, in turn, caused either the flame to accelerate, ignite a new deflagration, or initiate a detonation ahead of the flame. Furthermore, the optical thickness of the particle suspension controlled whether the radiative preheating triggers a deflagration or a detonation ahead of the flame.

In this paper we explore the effect of thermal radiation on layered dust explosions using fully compressible multidimensional numerical simulations. Scenarios where coal particles are initially placed on a thin layer on the floor of a long channel, as shown in Fig. 1, are considered. Similar to our earlier work (Houim and Oran, 2015b,c) and Shimura and Matsuo (2019), the shock remnant of a failed gas-phase detonation disperses the coal dust into the shock-heated air where particles ignite and burn. Unlike these prior works, the simulations here include the effect of thermal radiation.

# 2. Problem Description and Numerical Methods

## 2.1. Physical Model

The initial and boundary conditions for the simulations are shown in Fig. 1. The domain consists of a long two-dimensional channel 5 cm in height, with a 4-mm thick layer of coal placed on the bottom. Channel lengths of 10 m and 40 m were considered. All boundaries of the domain are assumed to be symmetry planes. The diameter of the coal particles is 30  $\mu$ m, which is in the size range for coal to produce dust explosions (Cashdollar, 2000). Volume fractions of 47% and 1% of particles in the dust layer were considered to explore the influence of particle packing. The 47% volume fraction of the dense cases is based on empirical data for loosely-packed coal dust layer (Edwards and Ford, 1988) and the dilute (1% volume fraction) cases are based on data from Semenov, Utkin and Markov (2013). The domain contains a stoichiometric mixture of methane and air from the left boundary up to 2 m. After 2 m, the rest of the domain is transitioned to pure air gradually, over a distance of about 1 m, using a hyperbolic tangent function. The dust explosion is initiated by igniting a methane-air detonation on the left portion of the domain. The detonation is triggered near the left boundary using two hot pockets of unreacted methane and air at 100 atm and 1000 K.

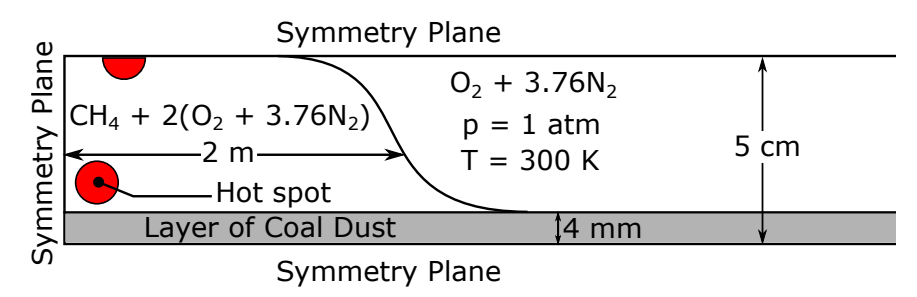


Figure 1: Initial and boundary conditions

The two-dimensional simulations are computed using an in-house code, HyBurn, which solves the full set of coupled, multiphase, compressible, unsteady, partial differential equations (Houim and Oran, 2016). Kinetic theory-based solid phase reactive multiphase equations are solved. Drag, convective heat transfer, particle-particle interactions and inelastic collisions are modeled (Houim and Oran, 2016). Details of the model and solution process can be found in Houim and Oran (2016) and Houim and Kuo (2011).

Magnus force is used to model the lift force, which is given by  $f_{\text{lift}} = C_l \alpha_s \rho_g(v_s - v_g) \times (\nabla \times v_g)$ , where  $C_l = 1$ . The lift coefficient was not varied in these simulations, since generally the shock-lifting of dust layers is insensitive to changes in it (Zydak and Klemens, 2007). Viscous stress, molecular diffusion, heat conduction and radiation are

all considered. The ideal gas model with variable specific heat is used to relate pressure, chemical composition, temperature and density of the gas phase. The gas phase is composed of CH<sub>4,g</sub>, O<sub>2</sub>, N<sub>2</sub>, H<sub>2</sub>O<sub>g</sub> and CO<sub>2</sub>. Global, irreversible reactions were used to model methane combustion in high speed flows from Cloney, Ripley, Pegg and Amyotte (2018), which is based on the MP1 model of CERFACS.

The dust particles are composed of dry ash-free coal (DAF), moisture ( $H_2O_s$ ), char ( $C_s$ ), and inert ash. The DAF is first assumed to devolatilize in a process based on Kobayashi, Howard and Sarofim (1977), releasing gaseous methane and solid carbon  $C_s$  (or char). The char can then react with air in a single-step process (Baek, Sichel and Kauffman, 1990). The moisture is allowed to vaporize based on an Arrhenius reaction (Bradley, Lawes, Park and Usta, 2006).

The particles are assumed to be spherical and monodisperse, with a diameter of 30  $\mu$ m, a constant specific heat of 987 J/kg.K, and material density,  $\rho_s$ , of 1200 kg/m<sup>3</sup> (Houim and Oran, 2015b). The coefficient of restitution used in these simulations is 0.99. The initial mass fractions of coal are 0.93 for DAF, 0.06 for ash, and 0.01 for moisture.

#### 2.2. Reaction Mechanism for the Gas and Solid Phases

The chemical reactions used in this paper are

$$DAF \xrightarrow{k_{DAF,1}} CH_4 + C_s, \tag{R1}$$

$$DAF \xrightarrow{k_{DAF,2}} CH_4 + C_s, \tag{R2}$$

$$H_2O_s \xrightarrow{k_{H_2O}} H_2O_g,$$
 (R3)

$$C_s + O_{2,g} \xrightarrow{k_{f(C)}} CO_2,$$
 (R4)

$$CH_4 + 2O_2 \xrightarrow{k_{CH_4}} CO_2 + 2H_2O.$$
 (R5)

The model of Kobayashi et al. (1977) is used for the devolatilization reactions where R1 is dominant a low temperatures and R2 is dominant at higher temperatures. The rate constants are

$$k_{\text{DAF 1}} = B_1 \exp(-E_1/RuT_p),$$
 (1)

$$k_{\text{DAF},2} = B_2 \exp(-E_2/RuT_p),\tag{2}$$

where Ru is the universal gas constant, the pre-exponential factors  $B_1$  and  $B_2$  are  $3.7 \times 10^5$  s<sup>-1</sup> and  $1.46 \times 10^{13}$  s<sup>-1</sup>, respectively, and activation energies  $E_1$  and  $E_2$  are  $7.37 \times 10^7$  J/mol and  $2.51 \times 10^8$  J/mol, respectively. The mass-based volatile yield fraction for R1 and R2 is 0.37 and 0.56, respectively.

Moisture vaporization, R3, is given as an Arrhenius reaction (Bradley et al., 2006) where

$$k_{\rm H_2O} = A_{\rm H_2O} \exp(-Ea_{\rm H_2O}/RuT_{\rm p}),$$
 (3)

and  $A_{\rm H_2O} = 1.46 \times 10^{13} \; {\rm s}^{-1}$  and  $Ea_{\rm H_2O} = 1.464 \times 10^8 \; {\rm J/mol.}$ 

The char reaction rate R4 is based on mixed diffusion-limited and chemical-kinetic limited combustion models where

$$\frac{1}{k_{f(C)}} = \frac{1}{k_{f(C), \text{ diff}}} + \frac{1}{k_{f(C), \text{ kin}}}.$$
(4)

The rate constant for the diffusion-limited char reaction is

$$k_{\rm f(C),\,diff} = \frac{24T_{\rm g}D_{\rm s}}{T_{\rm o} + T_{\rm p}},\tag{5}$$

where  $T_{\rm g}$  is gas temperature and  $D_{\rm s}=100~{\rm mm^2/s}$ , which is an averaged mass diffusivity of for the char reaction (Cloney et al., 2018). The chemical-kinetic limited rate constant is

$$k_{f(C), kin} = A_C \exp(-Ta_C/T_p), \tag{6}$$

where  $A_C = 9.5 \times 10^7 \text{ s}^{-1}$  and activation temperature is  $Ta_C = 17,977 \text{ K}$  (Baek et al., 1990).

The volatiles are assumed to be pure CH<sub>4</sub> and react with oxygen in a single-step irreversible reaction R5. The molar consumption rate is give by

$$\frac{d[CH_4]}{dt} = k_{\text{CH}_4}[CH_4]^1[O_2]^{1/2}.$$
 (7)

The rate constant is

$$k_{\text{CH}_4} = A_{\text{CH}_4} \exp(-Ea_{\text{CH}_4}/RuT), \tag{8}$$

where  $A_{CH_4} = 1.1 \times 10^{10} \sqrt{\rm g/s}$  is the pre-exponential factor and  $Ea_{CH_4} = 20,000$  cal/mol. Despite its simplicity, this single-step volatile combustion model has been shown to produce relatively good results for laminar coal dust flames (Clonev et al., 2018).

## 2.3. Thermodynamic and Transport Models

The fluid model uses a variable specific heats model to preserve a high degree of accuracy. The thermodynamic and transport data for the species have been obtained from the AramcoMech2.0 library. The transport properties are assumed to be mixture-average. A generic transport property  $\psi$  for the mixture is

$$\psi_{\text{mix}} = \left(\sum_{i=1}^{N_g} X_i \psi_i^{1/n}\right)^n, \tag{9}$$

where n is 1/6 for the mixture viscosity and 4 for the mixture thermal conductivity (Ern and Giovangigli, 1994).

The Curtis-Hirschfelder approximation is used for the mixture-averaged mass diffusion coefficients (Kee, Coltrin and Glarborg, 2005)

$$D_{i,mix} = \frac{1 - Y_i}{\sum_{i \neq i}^{N_g} X_j / D_{ij}},\tag{10}$$

where  $D_{ij}$  are the binary diffusion coefficients of all pairs of species. The correction procedure of Coffee and Hiemerl (Coffee and Heimerl, 1981) is used to ensure mass conservation for the diffusion velocities.

#### 2.4. Radiation Modeling

In this work we solve the radiation transfer equation (RTE) to compute the radiation field and the radiative heating and cooling rates for the particles. The RTE is given by

$$\frac{1}{c}\frac{\partial I}{\partial t} + \Omega \cdot \nabla I + \sigma_s I = \frac{1}{4\pi} \int_{4\pi} d\Omega' \sigma_s I(\mathbf{r}, \Omega') + \sigma_{a, \text{gas}} \left(\frac{acT_{\text{gas}}^4}{2\sqrt{\pi}} - I\right) + \sigma_{a, \text{particles}} \left(\frac{acT_{\text{particles}}^4}{2\sqrt{\pi}} - I\right), \quad (11)$$

where c is the speed of light, I is the radiation intensity,  $\Omega$  is the angular variable,  $\sigma_s$  is the scattering coefficient,  $\sigma_{a,\mathrm{gas}}$  and  $\sigma_{a,\mathrm{particles}}$  are the absorption coefficient for the gas and particle phases respectively, a is a radiation constant  $(1.372 \times 10^{13} \, \text{Jm}^{-3} \text{keV}^{-4})$ . The incident radiation is defined as

$$G = \int_{4\pi} I d\Omega, \tag{12}$$

and the radiation heat source can be written as

$$-\nabla \cdot q_{\text{rad,gas}} = \sigma_{a,\text{gas}}(G - 4\pi I_{b,\text{gas}}), \tag{13}$$

and

$$-\nabla \cdot q_{\text{rad,particles}} = \sigma_{a, \text{particles}}(G - 4\pi I_{b, \text{particles}}), \tag{14}$$

for the gas and particles respectively, where  $q_{\rm rad}$  is the radiative heat flux and  $I_b$  is the blackbody intensity.

The third-order filtered spherical harmonics (FP<sub>3</sub>) approximation is used to simplify the RTE (Radice, Abdikamalov, Rezzolla and Ott, 2013). The radiation is assumed to be spectrally gray with isotropic scattering. The Buckius and Hwang correlation is used to compute the Planck-mean extinction and scattering coefficients for the coal dust (Buckius and Hwang, 1980). The gray Plank-mean absorption coefficients for CH<sub>4</sub>, O<sub>2</sub>, CO<sub>2</sub> and H<sub>2</sub>O were based on curve fits to the data from the RADCAL program (Grosshandler, 1993).

#### 2.5. Numerical Solution Methods

An operator splitting method is used to solve the governing equations with separate solution methods for hydrodynamic terms, source terms aring from chemical reactions, drag, etc., and thermal radiation. The hydrodynamic terms are solved using a Godunov-based method and a third-order Runge-Kutta method is used for time integration (Houim and Kuo, 2011; Houim and Oran, 2016). The FP<sub>3</sub> equations are marched in pseudo-time until steady-state is achieved using an approximate Riemann solver (McClarren and Hauck, 2010). The gas-phase reaction terms are integrated in time using the yet-another-stiff-solver (YASS) method (Khokhlov, Domínguez, Bacon, Clifford, Baron, Hoeflich, Krisciunas, Suntzeff and Wang, 2012).

Adaptive mesh refinement was used to achieve the required amount of resolution, which is based on the AMReX library (Zhang, Almgren, Beckner, Bell, Blaschke, Chan, Day, Friesen, Gott, Graves, Katz, Myers, Nguyen, Nonaka, Rosso, Williams and Zingale, 2019). Four levels of refinement were used with finest resolution of  $\Delta x_{\text{max}} = 0.2 \text{ mm}$ , which is roughly 6.7 particle diameters in size. This computational cell size is comparable to the resolution used in our earlier work (Houim and Oran, 2015b).

We performed a wide range of verification tests. These tests include the dense and dilute granular shock tube tests from Houim and Oran (2016), a constant-volume reactor test for the gas-phase reaction mechanism, a laminar flame speed test, and a 2-D lattice test for the radiation model (Radice et al., 2013). Here, the details of the coal-dust flame speed test are discussed. The initial conditions for the coal-dust laminar flame speed test are shown in Fig. 2 (a). The right half of the channel is filled with a stoichiometric mixture of coal-dust (4  $\mu$ m diameter) and air at room temperature and with a dust concentration of ~144 g/m³, and the left half has high temperature products. Once ignited, the flame propagates to the right of the channel at a stable velocity known as the laminar flame speed,  $S_L$ , which was ~28 cm/s for our simulations. This value compares well to the numerical and experimental results from Cloney et al. (2018). The temperatures for both the phases and the major species mass fractions at ~98 ms shown in Fig. 2 (b) give us an idea of the overall flame structure.

The numerical methods and models have been used to simulate layered dust explosions (Houim and Oran, 2015a,b), dust dispersal by a shock wave (Ugarte, Houim and Oran, 2017), and our previous results compare well with laboratory-scale observations (Li, Kauffman and Sichel, 1995).

## 3. Results

#### 3.1. Short 10-m channel with 47% volume fraction in the dust layer

Fig. 3 shows position-time (X-t) diagrams for the short channel cases. These plots show the propagation of the detonation, its subsequent failure, propagation of the dust flame, and the reflection of the incident shock. The methaneair detonation fails at  $\sim$ 1.5 ms after it propagates into a region without any presuspended methane in the air. The resulting shock remnant and the dust flame propagate separately. The incident shock propagates to the right and reflects from the end wall at  $\sim$ 14 ms and propagates towards the flame. After failure of the detonation, the flame decelerates until the reflected shock reaches the flame front at  $\sim$ 22 ms. In the case with radiation, the dust flame accelerates to the right after the shock-flame interaction. The dust flame in the non-radiative case is much more unstable and does not accelerate to the right.

Fig. 4 (a) shows the heat release rates due to gas-phase chemical reactions for the cases with and without radiation. The heat release rate is  $\sim$ 2 GW/m for the first 1.5 ms which is due to the propagating detonation. The heat release rate then sharply falls after the detonation fails at 1.5 ms due to lack of pre-suspended CH<sub>4</sub> in the air beyond the first two meters in the channel. Shortly after the failure of the detonation, the heat release rate rises continuously until  $\sim$ 12 ms for both cases due to the propagating dust flame. A case with pure inert dust in the layer, does not show the continuous rise in the heat release after detonation failure as shown in Fig. 4 (b). The heat release rate increases substantially at  $\sim$ 30 ms, which is likely due to effects from the shock-flame interactions enhancing mixing. After  $\sim$ 36 ms, the heat

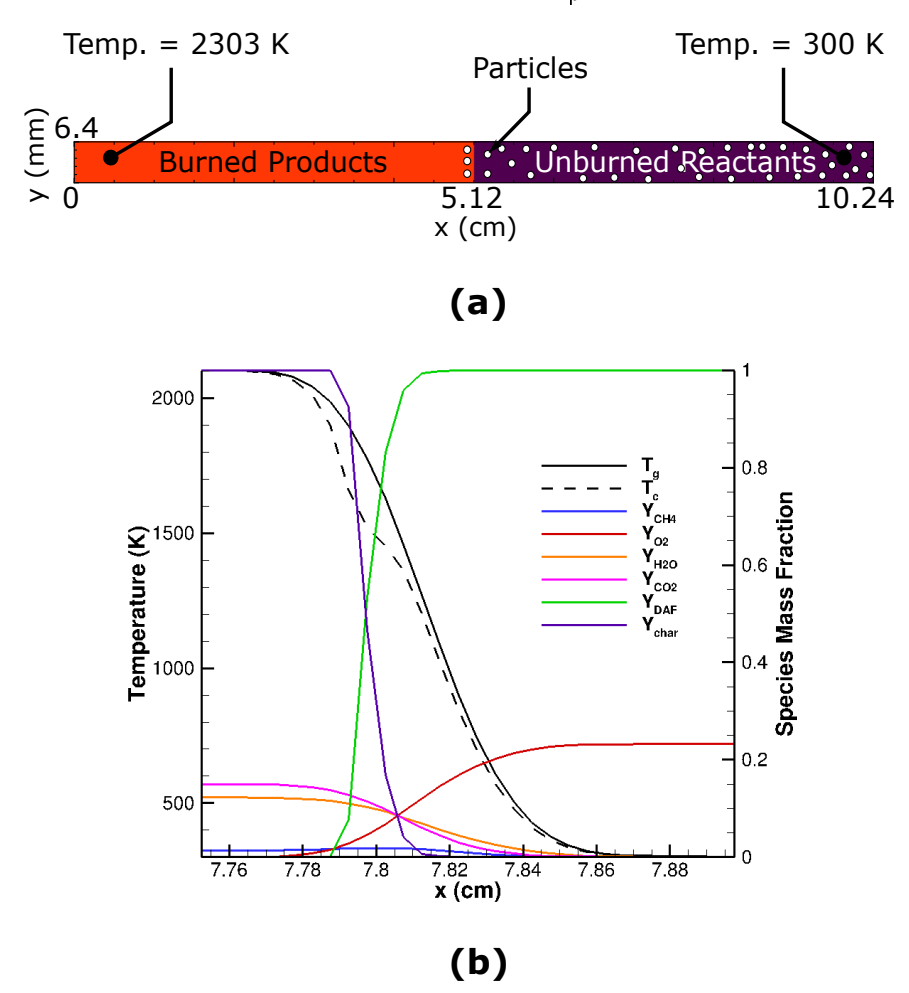


Figure 2: Laminar coal-dust flame speed test (a) initial conditions and configuration; (b) flame structure showing the gas-phase and granular-phase temperatures, and major species mass fraction plots.

release rate for the case without radiation decreases sharply and continuously until the end of the simulation while the case with radiation decreases more gradually and appears to be plateauing.

Fig. 5 shows a snapshot of the structure of the coal-dust flames for both cases at 45 ms. The radiative flame, at this instance, has a much broader structure and a lower peak temperature. The flame temperature predicted by the case without radiation at  $\sim 20$  ms is  $\sim 2250$  K, whereas for the case with radiation, it is  $\sim 2050$  K due to local radiative heat losses to the flame.

# 3.2. Long 40-m channel with 47% volume fraction in the dust layer

Reflected shocks interacted with the flame in the shorter 10-m channel cases. Longer 40-m long channels were simulated to eliminate the effect of these shock-flame interactions. Here we present the results for the long-channel cases with a dust layer volume fraction of 47%, with and without radiation. This case is nearly identical to setups discussed in Houim and Oran (2015c,b); Shimura and Matsuo (2019), but with a different reaction mechanism, different coal parameters, and a much longer simulation time.

The total heat release rates due to gas phase chemical reactions and the flame and shock velocities for these cases are shown in Fig. 6. Fig. 7 shows position-time (X-t) diagram of the temperature field at y = 2.5 cm. At ~80 ms, the heat release is substantially decreasing with and without radiation. In addition, the flame velocity, shown in Fig. 6(b), continuously decreases and eventually approaches zero. However, the flame locations and velocities are different for the two cases. At the end of the calculation ( $t \sim 80$  ms) the flame is at 11.0 m, and 9.9 m for for non-radiative and

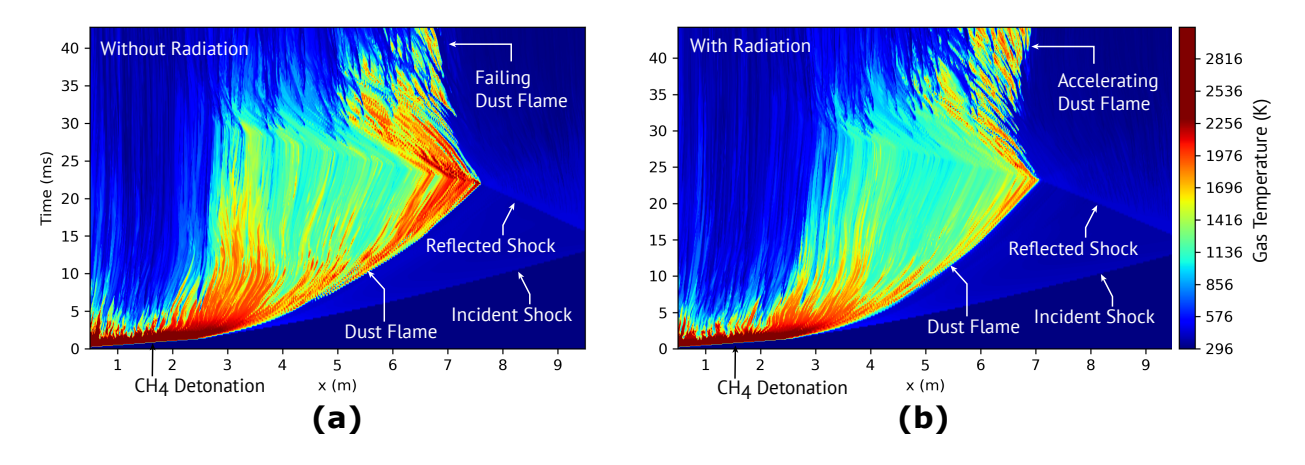


Figure 3: X-t diagram shaded by gas phase temperature for the 10-m channel with 47% layer volume fraction for (a) without radiation and (b) with radiation.

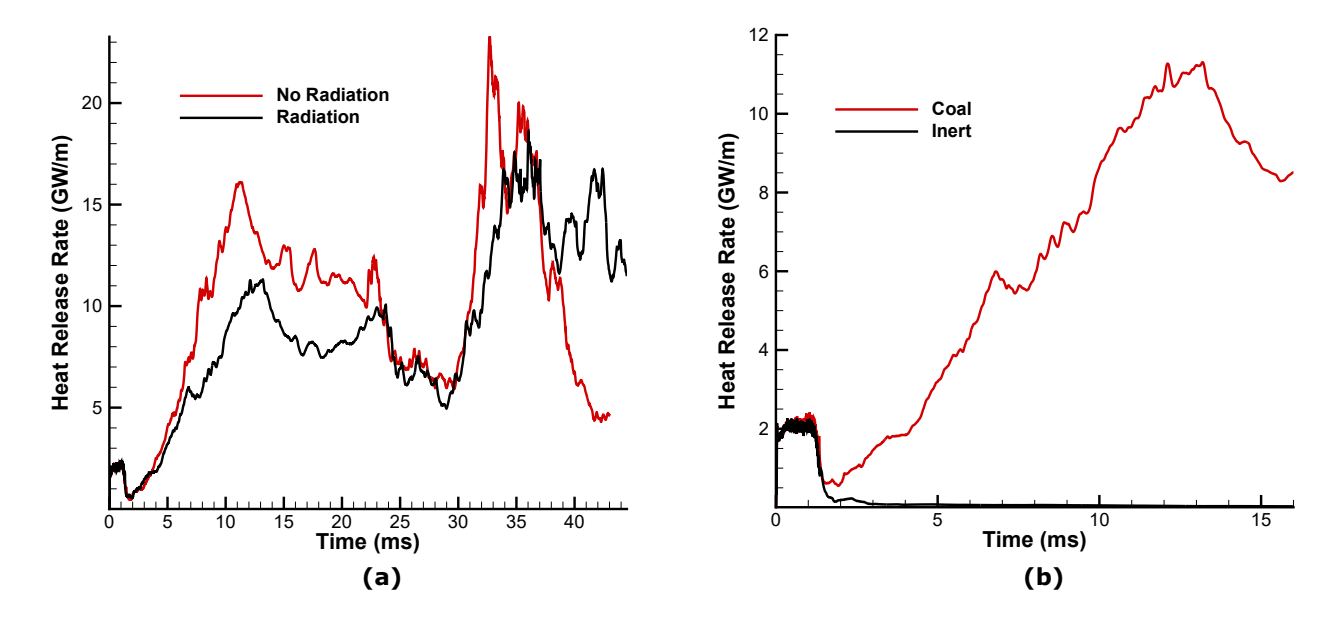


Figure 4: Heat release rates due to chemical reactions for the cases (a) with and without radiation; (b) with inert ash and reactive coal for the 10 m channel with a dust volume fraction of 47%.

radiative cases, respectively.

The X-t diagrams shown in Fig. 7 indicate that the peak coal dust flame temperature is around 200 K lower when radiation is considered. The dust flame starts to quench for the radiative case when the peak temperature drops to ~1200 K after 70 ms. The non-radiative flame shown in Fig. 7 (a) propagates unstably after 30 ms, with intermittent regions of high flame temperature followed by substantially lower temperatures.

## 3.3. Long channel with 1% volume fraction in the dust layer

The 40-m long channel was simulated with a volume fraction of 1% to explore the influence of dust layer packing on the simulation results. Note that such low volume fractions are not practical in coal mines. This case was studied only as an extreme scenario to understand the propagation and the fundamental differences between radiative and non-radiative cases better. Total heat release rate due to gas-phase chemical reactions and the shock and flame velocities are shown in Fig. 8(a) and (b), respectively. The heat release rate continually increases and the flame velocity propagates

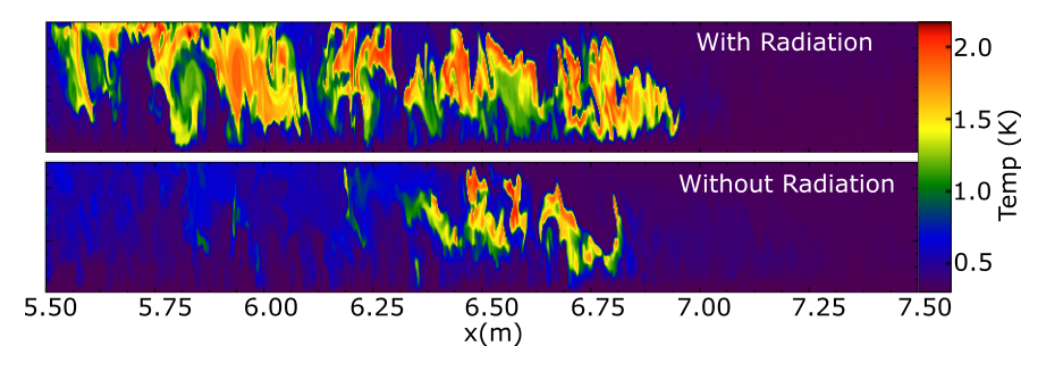


Figure 5: Contour plots of gas temperature for the cases with and without radiation at 45 ms for the 10-m channel the dust layer volume fraction fo 47%. Note that the plots have been stretched in the y-direction by 4 times for better visualization.

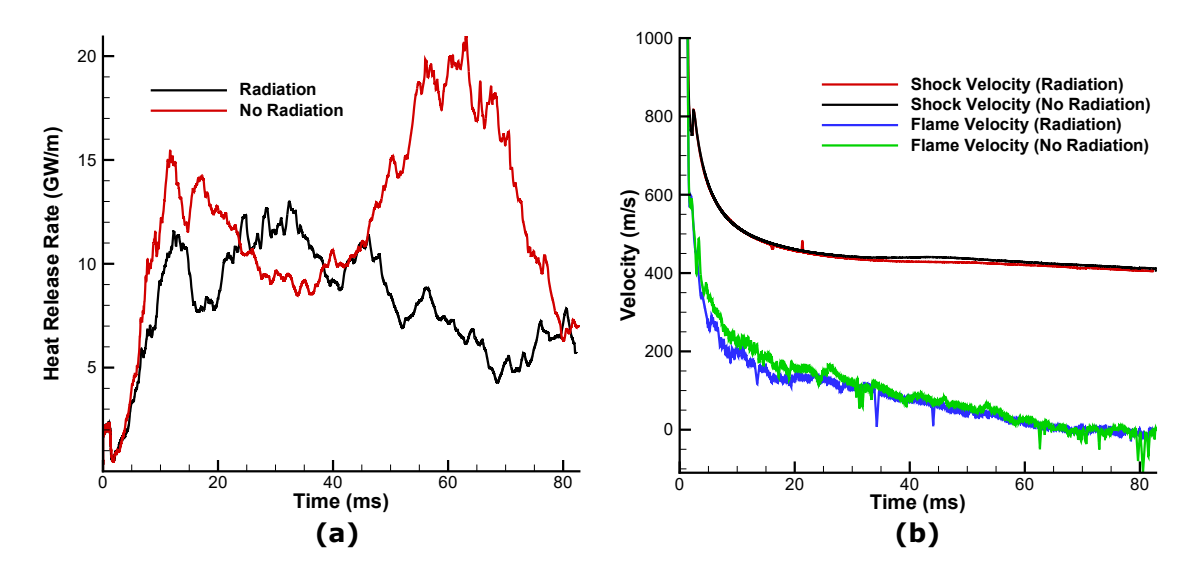


Figure 6: Results for the dense layer case (47% initial volume fraction) cases showing (a) total heat release rate due to gas phase chemical reactions and (b) shock and flame velocities.

stably at roughly 400 m/s for much of the calculation for these dilute cases. This is in contrast to the dense cases where the flames eventually quenched or propagated unstably.

The X-t diagram in Fig. 9 shows that thermal radiation is accelerating the flame, which is indicated by the slight kink in the flame position in Fig. 9(b), at  $\sim$ 50 ms. This corresponds to the time in Fig. 8(b) where the flame with radiation begins to accelerate relative to the case without radiation. It is interesting to note that the radiative flame produces higher peak flame temperatures relative to the non-radiative flame after 40 ms, which is opposite to the previous cases.

Fig. 10 shows the flame structure for (a) radiative case and (b) non-radiative case for the dilute dust layer. It is clear that radiation has an influence on the flame structure and temperature. In particular, the radiative case shows devolatilization over a longer distance ahead of the flame, which is indicative of radiative pre-heating.

#### 4. Discussion

The simulation results show that the influence of radiation on the bulk dust flame parameters, such as velocity and peak temperatures, are quite different for the scenarios presented in the paper and can even have opposite effects. For example, radiation hinders flame propagation in some cases, and assists propagation in other cases. The chemical energy release rate shown in Figs. 4, 6, and 8 show that for majority of the time in most cases the total rate of heat release is reduced by radiation. This trend can be explained by radiation losses from the flame region dominating

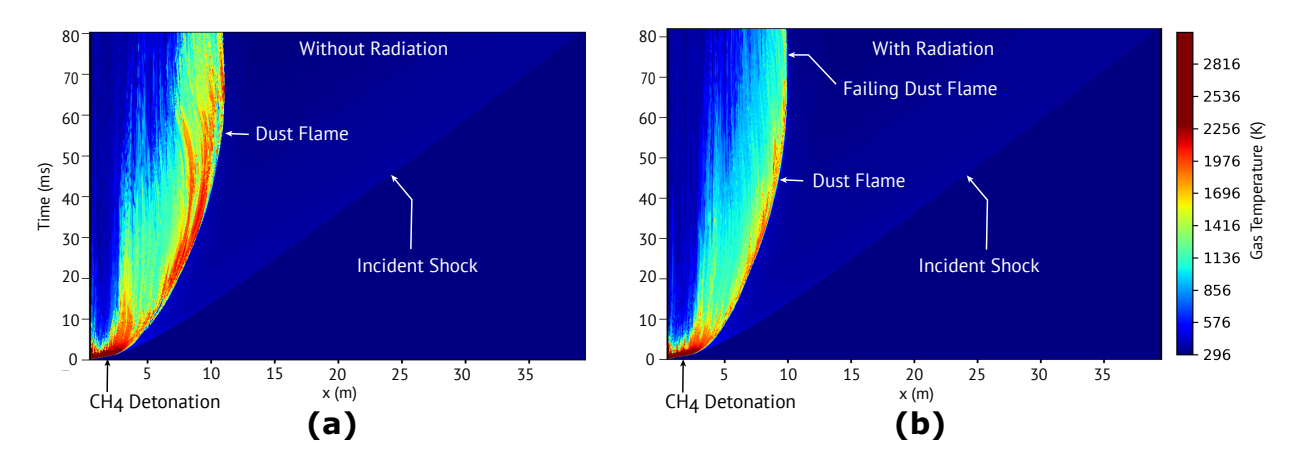


Figure 7: Dense (47% volume fraction) case X-t plot shaded by gas phase temperature for (a) without radiation and (b) with radiation.

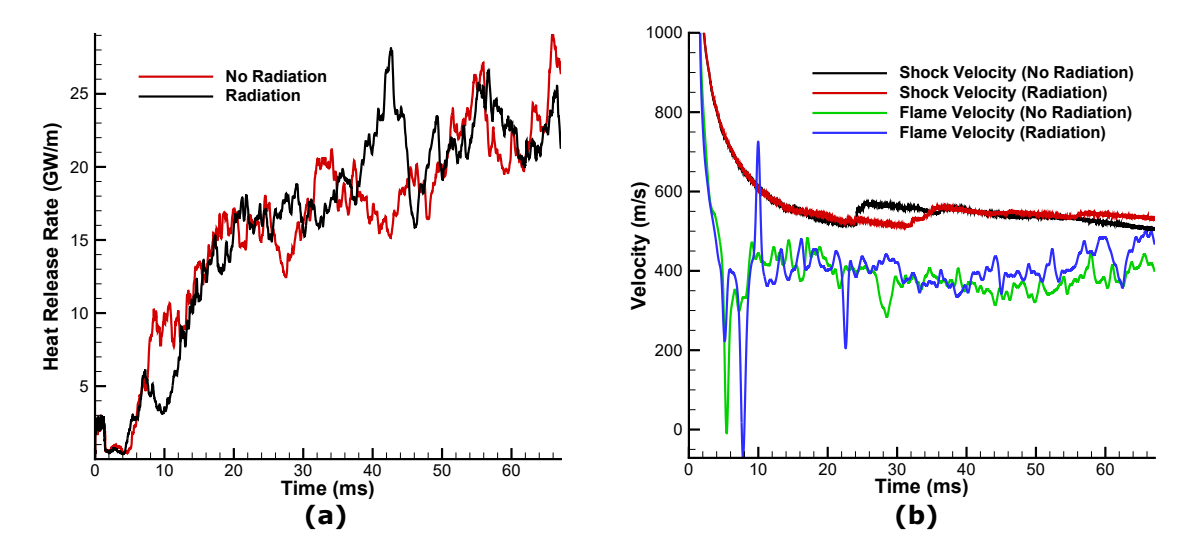


Figure 8: Dilute (1% volume fraction) case (a) Total heat release rate due to gas phase chemical reactions; (b) Shock and flame velocities

over radiation absorption in the cold reactants. These radiation losses near the flame reduce the peak temperature relative to the non-radiative simulations. A notable exception is the dilute cases where the opposite trend was observed. The radiative case with a layer volume fraction of 1% had peak flame temperatures that were  $\sim\!20$  K higher than the corresponding non-radiative case. This can be explain by the faster Mach 1.4 shock raising the air temperature by  $\sim\!20$  K for the radiative case compared to the Mach 1.33 shock for the non-radiative case. Another notable influence of radiation is that it produced a stably propagating flame for the shorter 10-m channel after the shock-flame interaction, while, simulations neglecting radiation produced a very unstable flame that is likely in process of quenching. This is shown most clearly in Figs. 3 and 5 which indicate a healthy flame for the radiative case and an unstable flame for the non-radiative case.

The flame is predicted to quench for both the radiative and non-radiative cases for the 40-m channel when a realistic layer volume fraction of 47% is used. Nevertheless, radiation has a significant influence on the quenching process. The radiative flame quenches much earlier than the non-radiative case due to radiation losses from flame overwhelming the radiative and conductive heating of the reactants. Quenching of the flame was an unexpected result that has not been

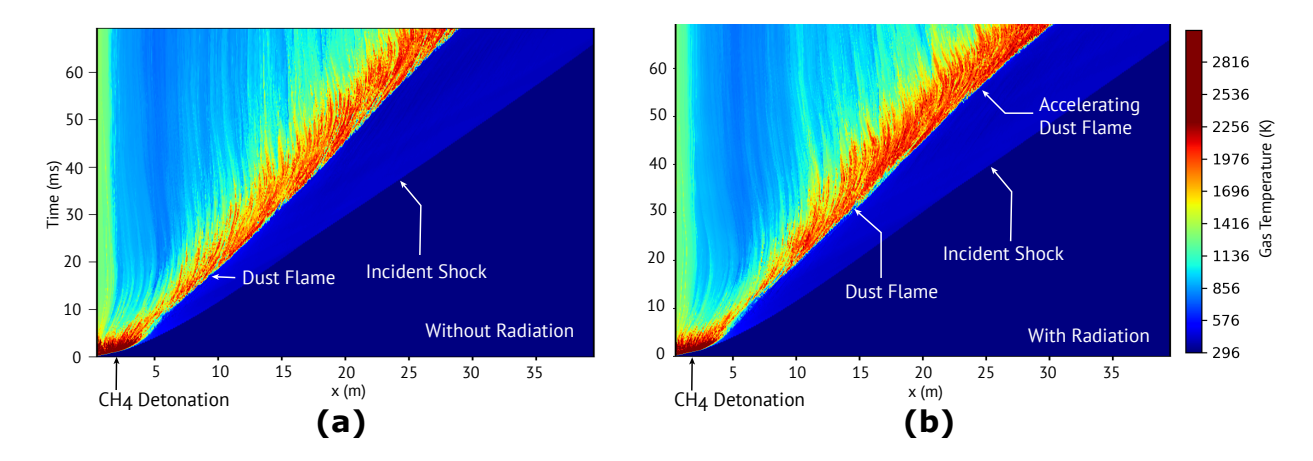


Figure 9: Dilute (1% volume fraction) case X-t plot shaded by gas phase temperature for (a) without radiation; (b) with radiation.

reported in earlier literature (Houim and Oran, 2015c; Shimura and Matsuo, 2019). However, these earlier simulations considered much shorter simulation times, used different reaction mechanisms for CH<sub>4</sub> and coal, and used different initial mass fractions for DAF, ash, and moisture. Exploring the sensitivity of the results to the choice in reaction mechanism and other model parameters is currently ongoing.

Flame velocities in the cases in which the flame propagates without quenching are within the experimentally determined range of 400-600 m/s that was reported in Sapko, Weiss, Cashdollar and Zlochower (2000).

## 5. Conclusions

Numerical simulations of layered coal dust explosions were performed both with and without radiation for 10 m and 40 m long channels to explore the influence of thermal radiation on the propagation of a layered dust explosion. Two particle volume fractions in the dust layer were considered. A loosely packed case with an 1% initial volume fraction and a densely packed case where the layer volume fraction was initially 47%. The results from the different cases were examined to understand the effect of radiation heat transfer on the structure and propagation of coal dust layered explosions.

The results of the simulations indicate that radiation can have a strong influence on layered dust explosions. Key dust flame parameters, such as flame temperature, velocity, and overall structure can be quite different between the radiative and non-radiative cases. However, the influence of radiation can have opposite effects for different scenarios. In some cases, radiation can lead to enhanced quenching of the explosion, while in others it can accelerate the flame and increase the severity of the explosion. For example, radiation promotes flame propagation after the reflected shockflame interaction in the 10-m channel, and for the dilute dust layer. However, radiation quenches the flame more quickly for the long channel with the dense dust layer. The precise conditions that lead to these differences are currently being explored.

The differences on the influence of radiation are likely dependent on modeling choice such as the chemical reaction model, spectral model for radiation, absorption and scattering models for the particles and gas, and other physical constant such as the lifting coefficient. Sensitivity of the results to these modeling choices is under investigation. We are currently performing simulations with similar configurations, but using detailed reaction mechanisms. We are also looking at the influence of particle size and spectral accuracy of the radiation model on the results. We will present these results in the future.

## 6. Acknowledgements

This work was supported in part by the US National Science Foundation (NSF) grant 1942861 and the US National Institute for Occupational Safety and Health (NIOSH) grant 200-2015-64091. The authors also would like thank

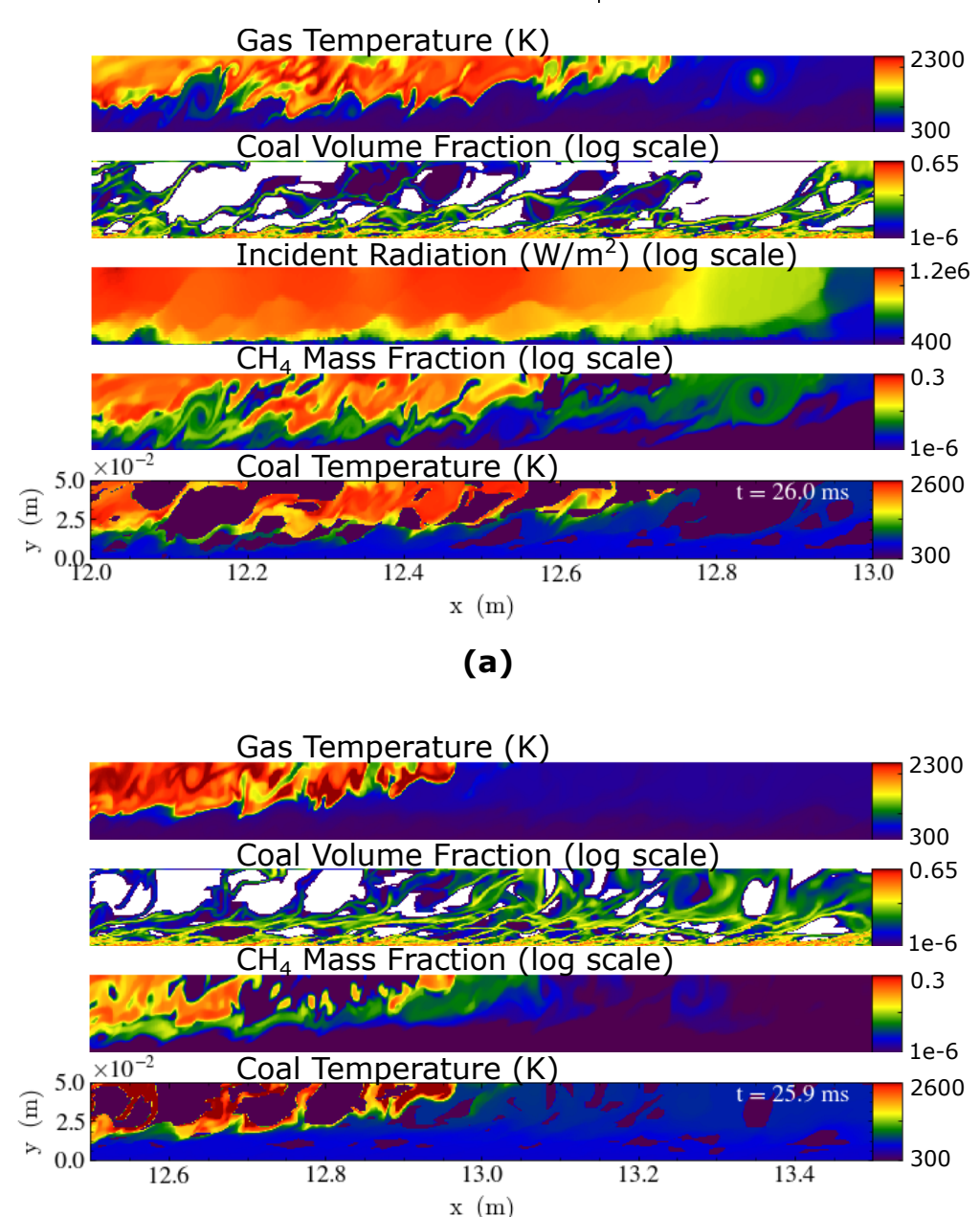


**Figure 10**: Plots of gas temperature, dust volume fraction, incident radiation, methane mass fraction, and coal temperature for cases (a) with radiation and (b) without radiation with the 1% volume fraction dust layer in the 40-m channel at a time of 26 ms.

(b)

Dr. Elaine Oran of Texas A&M and Marcia Harris and Dr. Mike Sapko of NIOSH for their fruitful discussions. The calculations presented in this paper were performed using the University of Florida high performance computing cluster, HiPerGator.

## References

- Baek, S., Sichel, M., Kauffman, C., 1990. Asymptotic analysis of the shock wave ignition of dust particles. Combustion and Flame 81, 219 228. URL: http://www.sciencedirect.com/science/article/pii/001021809090020R, doi:https://doi.org/10.1016/0010-2180(90)90020-R.
- Bidabadi, M., Azad, A.V., 2015. Effects of radiation on propagating spherical flames of dust-air mixtures. Powder Technology 276, 45 59. URL: http://www.sciencedirect.com/science/article/pii/S0032591014010262, doi:https://doi.org/10.1016/j.powtec.2014.12.044.
- Bradley, D., Lawes, M., Park, H.Y., Usta, N., 2006. Modeling of laminar pulverized coal flames with speciated devolatilization and comparisons with experiments. Combustion and Flame 144, 190 204. URL: http://www.sciencedirect.com/science/article/pii/S001021800500194X, doi:https://doi.org/10.1016/j.combustflame.2005.07.007.
- Buckius, R.O., Hwang, D.C., 1980. Radiation Properties for Polydispersions: Application to Coal. Journal of Heat Transfer 102, 99-103. URL: https://doi.org/10.1115/1.3244256, doi:10.1115/1.3244256, arXiv:https://asmedigitalcollection.asme.org/heattransfer/article-pdf/102/1/99/5909584/99\_1.pdf.
- Cao, W., Gao, W., Liang, J., Xu, S., Pan, F., 2014. Flame-propagation behavior and a dynamic model for the thermal-radiation effects in coal-dust explosions. Journal of Loss Prevention in the Process Industries 29, 65 71. URL: http://www.sciencedirect.com/science/article/pii/S0950423014000254, doi:https://doi.org/10.1016/j.jlp.2014.02.002.
- Cashdollar, K.L., 2000. Overview of dust explosibility characteristics. Journal of Loss Prevention in the Process Industries 13, 183 199. URL: http://www.sciencedirect.com/science/article/pii/S095042309900039X, doi:https://doi.org/10.1016/S0950-4230(99)
- Cloney, C.T., Ripley, R.C., Pegg, M.J., Amyotte, P.R., 2018. Laminar burning velocity and structure of coal dust flames using a unity lewis number cfd model. Combustion and Flame 190, 87 102. URL: http://www.sciencedirect.com/science/article/pii/S0010218017304492, doi:https://doi.org/10.1016/j.combustflame.2017.11.010.
- Coffee, T., Heimerl, J., 1981. Transport algorithms for premixed, laminar steady-state flames. Combustion and Flame 43, 273 289. URL: http://www.sciencedirect.com/science/article/pii/0010218081900274, doi:https://doi.org/10.1016/0010-2180(81)90027-4.
- Edwards, J., Ford, K., 1988. Model of coal-dust explosion suppression by rock dust entrainment. report of investigations/1988.
- Ern, A., Giovangigli, V., 1994. Multicomponent transport algorithms. volume 24. Springer Science & Business Media.
- Grosshandler, W.L., 1993. Radcal: a narrow-band model for radiation. Calculations in a Combustion Environment, NIST Technical Note 1402.
- Houim, R.W., Kuo, K.K., 2011. A low-dissipation and time-accurate method for compressible multi-component flow with variable specific heat ratios. Journal of Computational Physics 230, 8527 8553. URL: http://www.sciencedirect.com/science/article/pii/S0021999111004621, doi:https://doi.org/10.1016/j.jcp.2011.07.031.
- Houim, R.W., Oran, E.S., 2015a. Effect of radiation on the propagation of planar coal dust flames in air.
- Houim, R.W., Oran, E.S., 2015b. Numerical simulation of dilute and dense layered coal-dust explosions. Proceedings of the Combustion Institute 35, 2083 2090. URL: http://www.sciencedirect.com/science/article/pii/S1540748914001904, doi:https://doi.org/10.1016/j.proci.2014.06.032.
- Houim, R.W., Oran, E.S., 2015c. Structure and flame speed of dilute and dense layered coal-dust explosions. Journal of Loss Prevention in the Process Industries 36, 214 222. URL: http://www.sciencedirect.com/science/article/pii/S0950423015000169, doi:https://doi.org/10.1016/j.jlp.2015.01.015.
- Houim, R.W., Oran, E.S., 2016. A multiphase model for compressible granular–gaseous flows: formulation and initial tests. Journal of Fluid Mechanics 789, 166–220. doi:10.1017/jfm.2015.728.
- Kee, R.J., Coltrin, M.E., Glarborg, P., 2005. Chemically reacting flow: theory and practice. John Wiley & Sons.
- Khokhlov, A., Domínguez, I., Bacon, C., Clifford, B., Baron, E., Hoeflich, P., Krisciunas, K., Suntzeff, N., Wang, L., 2012. Three-dimensional simulations of thermonuclear detonation with alpha-network: Numerical method and preliminary results, in: Advances in Computational Astrophysics: Methods, Tools, and Outcome, p. 107.
- Kobayashi, H., Howard, J., Sarofim, A., 1977. Coal devolatilization at high temperatures. Symposium (International) on Combustion 16, 411-425. URL: http://www.sciencedirect.com/science/article/pii/S008207847780341X, doi:https://doi.org/10.1016/S0082-0784(77)80341-X.
- Li, Y.C., Kauffman, C., Sichel, M., 1995. An experimental study of deflagration to detonation transition supported by dust layers. Combustion and Flame 100, 505-515. URL: https://www.sciencedirect.com/science/article/pii/001021809400142F, doi:https://doi.org/10.1016/0010-2180(94)00142-F. 25th Symposium (International) on Combustion Papers.
- Liberman, M., Ivanov, M., Kiverin, A., 2015. Effects of thermal radiation heat transfer on flame acceleration and transition to detonation in particle-cloud hydrogen flames. Journal of Loss Prevention in the Process Industries 38, 176 186. URL: http://www.sciencedirect.com/science/article/pii/S0950423015300310, doi:https://doi.org/10.1016/j.jlp.2015.09.006.
- McClarren, R.G., Hauck, C.D., 2010. Robust and accurate filtered spherical harmonics expansions for radiative transfer. Journal of Computational Physics 229, 5597 5614. URL: http://www.sciencedirect.com/science/article/pii/S0021999110001622, doi:https://doi.org/10.1016/j.jcp.2010.03.043.
- Radice, D., Abdikamalov, E., Rezzolla, L., Ott, C.D., 2013. A new spherical harmonics scheme for multi-dimensional radiation transport i. static matter configurations. Journal of Computational Physics 242, 648 669. URL: http://www.sciencedirect.com/science/article/pii/S0021999113001125, doi:https://doi.org/10.1016/j.jcp.2013.01.048.
- Sapko, M.J., Weiss, E.S., Cashdollar, K.L., Zlochower, I.A., 2000. Experimental mine and laboratory dust explosion research at niosh. Journal of Loss Prevention in the Process Industries 13, 229 242. URL: http://www.sciencedirect.com/science/article/pii/S0950423099000388, doi:https://doi.org/10.1016/S0950-4230(99)00038-8.
- Semenov, I., Utkin, P., Markov, V., 2013. Numerical modelling of dust-layered detonation structure in a narrow tube. Journal of Loss Prevention in the Process Industries 26, 380 386. URL: http://www.sciencedirect.com/science/article/pii/S0950423012000605, doi:https:

#### Radiation effects on Dust Explosions

- //doi.org/10.1016/j.jlp.2012.04.007. selected Papers from the Eighth International Symposium on Hazards, Prevention, and Mitigation of Industrial Explosions (Yokohama, Japan, 5–10 September 2010).
- Shimura, K., Matsuo, A., 2019. Using an extended cfd-dem for the two-dimensional simulation of shock-induced layered coal-dust combustion in a narrow channel. Proceedings of the Combustion Institute 37, 3677 3684. URL: http://www.sciencedirect.com/science/article/pii/S154074891830484X, doi:https://doi.org/10.1016/j.proci.2018.07.066.
- Slezak, S.E., Buckius, R.O., Krier, H., 1985. A model of flame propagation in rich mixtures of coal dust in air. Combustion and Flame 59, 251 265. URL: http://www.sciencedirect.com/science/article/pii/0010218085901294, doi:https://doi.org/10.1016/0010-2180(85)90129-4.
- Ugarte, O.J., Houim, R.W., Oran, E.S., 2017. Examination of the forces controlling dust dispersion by shock waves. Phys. Rev. Fluids 2, 074304. URL: https://link.aps.org/doi/10.1103/PhysRevFluids.2.074304, doi:10.1103/PhysRevFluids.2.074304.
- Zhang, W., Almgren, A., Beckner, V., Bell, J., Blaschke, J., Chan, C., Day, M., Friesen, B., Gott, K., Graves, D., Katz, M., Myers, A., Nguyen, T., Nonaka, A., Rosso, M., Williams, S., Zingale, M., 2019. Amrex: a framework for block-structured adaptive mesh refinement. Journal of Open Source Software 4. doi:10.21105/joss.01370.
- Zydak, P., Klemens, R., 2007. Modelling of dust lifting process behind propagating shock wave. Journal of Loss Prevention in the Process Industries 20, 417 426. URL: http://www.sciencedirect.com/science/article/pii/S0950423007000691, doi:https://doi.org/10.1016/j.jlp.2007.04.020. selected Papers Presented at the Sixth International Symposium on Hazards, Prevention and Mitigation of Industrial Explosions.